Cell, Vol. 114, 135–146, July 11, 2003, Copyright ©2003 by Cell Press

Structure of the Rho Transcription Terminator: Mechanism of mRNA Recognition and Helicase Loading

Emmanuel Skordalakes and James M. Berger*
Department of Molecular and Cell Biology
University of California, Berkeley
239 Hildebrand Hall, #3206
Berkeley, California 94720

Summary

In bacteria, one of the major transcriptional termination mechanisms requires a RNA/DNA helicase known as the Rho factor. We have determined two structures of Rho complexed with nucleic acid recognition site mimics in both free and nucleotide bound states to 3.0 Å resolution. Both structures show that Rho forms a hexameric ring in which two RNA binding sites—a primary one responsible for target mRNA recognition and a secondary one required for mRNA translocation and unwinding—point toward the center of the ring. Rather than forming a closed ring, the Rho hexamer is split open, resembling a "lock washer" in its global architecture. The distance between subunits at the opening is sufficiently wide (12 Å) to accommodate single-stranded RNA. This open configuration most likely resembles a state poised to load onto mRNA and suggests how related ring-shaped enzymes may be breached to bind nucleic acids.

Introduction

Appropriate termination of transcription is essential for proper regulation of gene expression. In bacteria, mRNA transcription termination is carried out by two distinct mechanisms (Richardson and Greenblatt, 1996). In intrinsic termination, an mRNA stem loop structure is thought to induce RNA polymerase to pause, promoting the release of both the polymerase and the RNA transcript from the template DNA. This mechanism accounts for approximately half of the termination sites in *Escherichia coli*, and resembles the transcription termination mechanism used by eukaryotic pol III. In contrast, the second mechanism of transcription termination is protein mediated and relies on an enzyme found throughout bacteria known as the Rho factor (Brown et al., 1981; Opperman and Richardson, 1994).

Since its discovery in 1969 by Roberts (Roberts, 1969), Rho has become a paradigm for understanding how exogenous proteins can regulate the termination of transcription by RNA polymerase. In vivo, Rho loads onto mRNAs at a cytosine-rich region of 40 or more bases known as a Rho utilization (*rut*) site (Morgan et al., 1985; Alifano et al., 1991). Once bound, Rho acts as a hexameric, 5′→3′ ATP-dependent helicase to translocate to the site of transcription and disengage the polymerase (Oda and Takanami, 1972; Lowery-Goldhammer and Richardson, 1974; Morgan et al., 1983; Brennan et al., 1987; Richardson, 2002). Rho can be regulated during this process by a number of factors, such as NusG, which serve as antiterminators to ameliorate the termination properties of the enzyme (Sullivan and Gottesman, 1992).

Tethering of Rho to a *rut* site is independent of ATP binding and/or hydrolysis (Galluppi and Richardson, 1980; McSwiggen et al., 1988) and is mediated by an N-terminal domain in each protomer of the Rho hexamer (Martinez et al., 1996a, 1996b; Allison et al., 1998; Briercheck et al., 1998). Previous high-resolution NMR and X-ray crystal structures of the N-terminal mRNA binding domain of Rho have provided a structural view of this fold and its interactions with target substrates (Allison et al., 1998; Briercheck et al., 1998; Bogden et al., 1999). The domain consists of a three-helix bundle that rests on top of a five-stranded β barrel. The barrel belongs to the oligonucleotide/oligossacharide binding (OB) protein superfamily and is primarily responsible for Rho's preferential interaction with cytosine-rich nucleic acids (McSwiggen et al., 1988; Geiselmann et al., 1992; Richardson and Richardson, 1992; Modrak and Richardson, 1994; Platt, 1994). Curiously, the domain does not specifically recognize the 2′-hydroxyl of RNA and can associate with ssDNA in vitro, a property that has been used to great effect for dissecting Rho function (Oda and Takanami, 1972; Richardson, 1982; Brennan et al., 1987).

The C-terminal region of Rho contains signature sequence motifs that are hallmarks of Walker-type ATP binding proteins. The closest homolog to Rho is the F_1 ATP synthase, an $\alpha_3\beta_3$ heterohexameric complex that assembles into rings and generates ATP from a protonmotive force (Boyer, 1997). Consistent with this relationship, EM studies have shown that Rho also forms hexameric rings, although in the absence of RNA, these rings exist in both closed and "notched" open forms (Oda and Takanami, 1972; Gogol et al., 1991; Yu et al., 2000). Notched rings have been interpreted either to be missing a subunit or to be a natural functional state of the protein for loading RNA into the hole of the hexamer (Yu et al., 2000). Open Rho rings can be converted into the closed form by the binding of extended single-stranded nucleic acids, which have been proposed to wrap around the perimeter of the hexamer (Galluppi and Richardson, 1980; McSwiggen et al., 1988; Gan and Richardson, 1999; Yu et al., 2000).

As Rho loads onto nascent mRNAs, the single-stranded substrate is thought to bind in the hole of the hexameric ring, where it interacts with a secondary RNA binding site in the C-terminal domains (Burgess and Richardson, 2001a; Burgess and Richardson, 2001b). Two regions, the Q and R loops, have been implicated in RNA associations at the secondary site (Miwa et al., 1995; Burgess and Richardson, 2001a; Wei and Richardson, 2001b), and RNA binding in the hole of the hexameric ring can stimulate ring closure when the secondary sites become affixed to the message (Gogol et al., 1991; Yu et al., 2000). After loading appropriately, the C-terminal domains are thought to engage in cycles of ATP binding and hydrolysis, translocating Rho along the mRNA until it reaches RNA polymerase and unwinds

*Correspondence: jmberger@uclink4.berkeley.edu

the RNA/DNA heteroduplex at the site of transcription (Lowery-Goldhammer and Richardson, 1974; Brennan et al., 1987, 1990; Walstrom et al., 1997; Burgess and Richardson, 2001a; Kim and Patel, 2001; Stitt, 2001). Two models have been advanced to describe the physical nature of the translocation/unwinding reactions (Richardson, 2002; Delagoutte and von Hippel, 2003). In one, known as the tethered tracking mechanism, Rho is thought to remain attached to the *rut* site while translocating toward the 3′ end of the mRNA (Steinmetz and Platt, 1994). In the other model, Rho is thought to detach from the *rut* site upon the onset of translocation (Geiselmann et al., 1993; von Hippel and Delagoutte, 2001).

Despite extensive efforts, several questions regarding the mechanism of Rho remain unanswered. For example, it is not known how the primary and secondary RNA binding sites are oriented with respect to each other, and whether this arrangement can accommodate the simultaneous RNA binding events predicted by the tethered tracking model. It has also remained unclear how an extended nucleic acid segment gains entry into the topologically closed-ring system of the Rho particle, a problem that exists for a variety of hexameric helicases.

To begin to address these questions, we determined the structure of the full-length *Escherichia coli* Rho protein bound to an ssDNA recognition site mimic to 3.0 Å resolution. The same structure bound to ssRNA and the ATP analog AMPPNP (adenosine 5′-(β,γ-imido)triphosphate) was also determined to 3.0 Å resolution. Both structures show that Rho forms hexameric rings in which the primary RNA binding sites of the N-terminal domains face toward the interior of the particle, positioning the 3′ end of nucleic acid exiting from the *rut*-recognition surface directly toward the hole of the hexamer. Nucleotide binds in a crevice between the C-terminal domains of neighboring protomers and is liganded by residues of the Walker-A and -B motifs. Secondary RNA binding motifs, which comprise the acceptor sites for translocating along RNA, line the perimeter of the interior hole: six Q loops together form a narrow constriction in the center of the ring, while each R loop lies above the P loop of the Walker-A motif. Strikingly, the Rho ring is split open in both the AMPPNP bound and unbound states, adopting an architecture akin to that of a lock washer. Taken together, these structural features illuminate the mechanism by which Rho associates with *rut* sites and loads the 3′ end of the mRNA into the interior of the ring prior to the start of translocation.

Results and Discussion

The Rho Monomer Structure

The full-length Rho protein used for these studies is hexameric in solution, as judged by both gel filtration and dynamic light scattering (data not shown). Although preliminary crystals of the purified protein grew readily, extensive optimization of initial crystallization conditions was required to obtain crystals that diffracted to a useful resolution. The key elements in this process proved to be cocrystallization of the protein with mild detergents and the use of an appropriate length and sequence of nucleic acid substrate. In all, two different Rho structures were obtained: one in complex with ssDNA and another bound to ssRNA and AMPPNP. The ssDNA-Rho complex was phased to intermediate resolution (6.0 Å) by single isomorphous replacement from a tantalum bromide derivative, followed by high-resolution phasing using selenomethionine-based MAD. The ssRNA/AMPPNP assembly was solved by molecular replacement. Both structures were refined to 3.0 Å resolution (Tables 1 and 2).

The crystalline asymmetric unit contains six Rho protomers assembled into a discrete hexameric particle. Each subunit is peanut-shaped, with dimensions of 65 Å in height, 50 Å in depth, and 35 Å in width (Figure 1A), and is composed of an N- and C-terminal domain joined together by an extended 30 residue linker. Although there is clear electron density for five out of six N-terminal domains in the hexamer, the N-terminal domain of protomer B is partially disordered, and electron density can only be seen for its C-terminal half.

The Rho N-terminal domain consists of two subdomains: a three-helix bundle followed by a five-stranded β barrel (Figure 1A). The β barrel is an OB-type fold, which is found in a wide variety of single-stranded nucleic acid binding molecules that include proteins such as type II aminoacyl tRNA synthases and cold shock proteins (Cavarelli et al., 1993; Newkirk et al., 1994; Schindelin et al., 1994). An indented face on one side of this subdomain forms the primary RNA binding site of Rho (Modrak and Richardson, 1994; Briercheck et al., 1998; Bogden et al., 1999). Structural comparisons of either the helical-bundle or the OB-fold subdomains between different protomers and isolated Rho N-terminal domains solved previously by NMR and X-ray crystallography show that the individual structures of these segments do not vary greatly (Cα RMSD 0.73Å) (Allison et al., 1998; Briercheck et al., 1998; Bogden et al., 1999). However, when comparing both subdomains in unison, the overall RMSDs for the entire N-terminal domain become higher (Cα RMSD 1.1Å) due to small variations in the relative orientations between the helical bundle and the OB fold. In the Rho hexamer, these differences are most prominent for protomers A and F.

Each of the six C-terminal domains of Rho consists of seven parallel β strands (β6–β13) sandwiched between several α helices (Figure 1A). There is clear electron density for residues 155–417 in all six C-terminal domains, although the last 15 residues exhibit higher than average temperature factors than the rest of the model. The average Cα RMSD between each of the six monomers in the hexamer is 0.58 Å. As expected from sequence analysis, the fold of the C-terminal domain belongs to the RecA superfamily of ATP binding proteins. A structural survey of such folds in the database shows that this region of Rho is most similar to the mitochondrial F_1 ATPase (Cα RMSD 2.1 Å) (Abrahams et al., 1994; Bird et al., 1998b).

There are several key signature sequence motifs located in the Rho C-terminal domain. One is the P loop, which is part of the Walker-A motif found in all RecA-family ATPases and is required for ATP binding and hydrolysis. Each P loop is formed by the β6/α7 connector segment and is juxtaposed with an adjacent protomer. A second important motif in Rho's C-terminal domain is the R loop, which connects the secondary structural elements β11/α12 and is located just below

Table 1. Data Collection and Phasing Statistics

	Rho-DNA Complex	Rho-RNA Complex	$Ta_6Br_{12}^{2+}$	Se-λ1	Se-λ2
Data set (λ Å)			1.245	1.0	0.9794
Resolution (Å)	50–3.0	50–3.0	50–4.6	50–3.6	50–3.6
Completeness (%)	97.9 (97.8)	96.1 (95.0)	95.7 (99.1)	94.3 (94.8)	96.2 (96.7)
Redundancy	2.2 (2.2)	2.2 (2.2)	2.5 (2.5)	2.3 (2.3)	2.3 (2.3)
R_{sym} (%)[a]	4.6 (27.2)	5.0 (33.2)	6.9 (30.4)	6.3 (24.5)	6.7 (29.4)
I/σ	15.5 (3.5)	15.3 (2.5)	10.0 (3.0)	12.9 (5.0)	11 (4.5)
Phasing Analysis			$Ta_6Br_{12}^{2+}$		Se
Resolution (Å)			20–6.0		20–3.6
R_{cullis} (%,acent/cent, iso)[b]			0.78/0.68		0.43/0.40
R_{cullis} (%, anom)[b]			0.80		0.78
Number of sites			6		83
Mean figure of merit (FOM)			0.432		0.308

Values in parentheses are for the highest-resolution bin.
[a] $R_{sym} = \Sigma\Sigma_j|I_j - \langle I\rangle|/\Sigma\langle I\rangle$, where I_j is the recorded intensity of the reflection j and $\langle I\rangle$ is the mean recorded intensity over multiple recordings.
[b] $R_{Cullis} = \Sigma\Sigma||F_{PH} \pm F_P| - F_H|/\Sigma|F_{PH} \pm F_P|$, where F_P and F_{PH} are the structure amplitudes of the parent and the heavy-atom derivative and F_H is the calculated heavy-atom structure factor.

the P loop. A third motif, the Q loop, is formed by an 8 residue segment that projects toward the center of the hexamer. Together, the Q and R loops are thought to form Rho's secondary RNA binding site (Burgess and Richardson, 2001a; Wei and Richardson, 2001a, 2001b; Xu et al., 2002).

The Rho Assembly

The six subunits of Rho pack laterally into a hexameric ring (Figures 2A and 2B). Subunit-subunit interactions occur between both the N- and C-terminal domains of each protomer. Contacts between adjacent N-terminal domains are generated between the α2/α3 connector loop in the helical bundle of one protomer and the extended linker that joins the N- and C-terminal domains of the adjacent subunit. In the C-terminal domain, α11 in one protomer packs against the β7/α8 and β8/α9 junctions of the neighboring subunit. The connector loop for secondary elements β11/α12 is also located at the C-terminal subunit-subunit interface and is positioned adjacent to and above the P loop of the ATP binding site.

Strikingly, the Rho ring is split open, giving rise to a global structure reminiscent of a lock washer (Figures 2A and 2B). This conformation is unusual, because nearly all full-length, ring-shaped ATPases observed crystallographically to date have been imaged with their rings closed. Open configurations of oligomeric ATPases have been observed previously for only a few proteins, including the recombination protein RecA and a truncated form of the bacteriophage T7 gp4 primase/helicase (Story et al., 1992; Sawaya et al., 1999). However, the particles in these structures do not exist as discrete hexamers and instead assemble into continuous filaments with 6_1 symmetry. EM analyses have shown that Rho hexamers are able to individually form both open and closed rings (Oda and Takanami, 1972; Gogol et al., 1991; Yu et al., 2000), although the purpose, function, and oligomeric organization of the open conformation have remained somewhat enigmatic. Our ability to trap and image an open conformation reminiscent of that seen previously by EM now suggests that this conformation is a stable and natural form accessed by the protein.

The diameter of the Rho ring is 120 Å, with a large interior hole that varies in width from 20–35 Å. The widest point of the hole is defined by the perimeter of the N-terminal domains, while the most narrow constriction is formed by the Q loop signature sequence motifs. The lock-washer arrangement of the hexamer arises from an upward rotation of one protomer with respect to

Table 2. Model Refinement

	Rho-DNA Complex	Rho-RNA Complex
Resolution (Å)	20–3.0	20–3.0
R_{free} (%)[a]	29.6	30.3
R_{work} (%)[b]	27.0	27.0
$RMSD_{bond}$ (Å)	0.014	0.010
$RMSD_{angle}$ (°)	1.47	1.25
Favored	85.6	84.6
Additionally allowed	12.4	13.2
Generously allowed	1.5	1.7
Total atoms (protein)	18,881	18,881
Total atoms (substrates)	190	386
Total atoms (Water)	20	15

[a] R_{free} is the R value calculated for a test set of reflections, comprising a randomly selected 5% of the data that is not used during refinement.
[b] $R_{work, free} = \Sigma||F_{obs}| - |F_{calc}||/|F_{obs}|$.

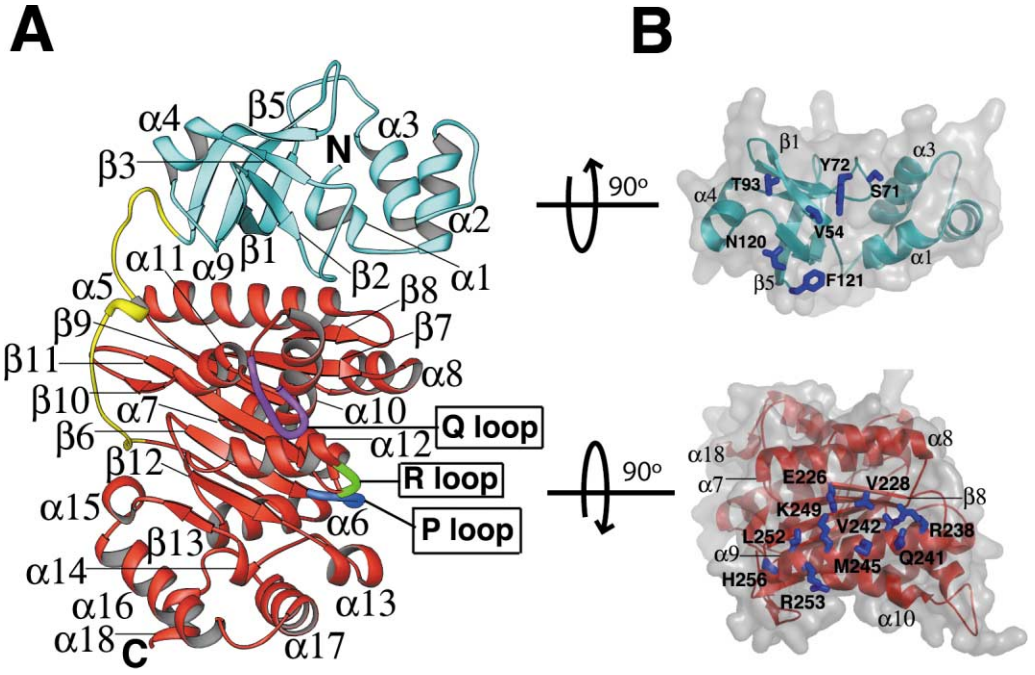

Figure 1. Structure and Topology of the Rho Protomer

(A) Structure of Rho protomer-D showing the relative orientations of the N- (cyan) and C- (red) terminal domains. Each N-terminal domain consists of a helical bundle and an OB-fold subdomain. The C-terminal domain is connected to the N-terminal domain by an extended linker (yellow) and consists of a RecA-type ATPase binding fold followed by a small helical subdomain. The P loop (blue), the Q loop (magenta), and the R loop (green) are highlighted. Secondary structure elements are labeled.

(B) Exploded views of the N- and C-terminal domain interface. Both domains are rotated by 90° opposite to each other. Residues involved in interdomain contacts are shown as blue rods and labeled.

another by approximately 15° about an axis that lies in a plane perpendicular to the pseudo 6-fold rotation axis of symmetry (Figure 2C). This swivel generates a helical rise of approximately ~8.5 Å along the rotational axis of the particle. By propagating these displacements about the ring of the hexamer, the midpoints of protomers A and F at either end of the ring are offset from each other by 45 Å, giving rise to a 12 Å wide gap that breaches the ring and allows access to the interior of the particle (Figure 2). It is interesting to note that the width of this gap is sufficient to allow for the entry of a single-stranded nucleic acid into the hole of the hexamer.

The intersubunit angular rise present in the Rho complex (15°) is within a range seen for the related ATPases RecA and T7 gp4. In RecA, however, the subunit-subunit rocking angle is more extreme and along the 6_1 helical axis (18°), which leads to filamentous assembly of the protein (Story et al., 1992). In contrast, for T7 gp4, two intersubunit rotation angles of 15° in the plane of the ring are offset by a downward 30° swing every third subunit that leads to ring closure (Singleton et al., 2000). Modulation of subunit-subunit orientations in these proteins is thought to occur in response to the combined action of ATP turnover and nucleic acid associations, which drive either strand exchange (RecA) or DNA translocation and unwinding (T7 gp4). In Rho, it appears that this common hinging mechanism has been further coopted to allow the protein to enter a ring-open conformation without perturbing the oligomerization state of the protein. Because the interior of Rho is capable of associating with mRNA in the absence of accessory factors (Burgess and Richardson, 2001a, 2001b), this structural organization appears consistent with a particle state competent to load onto extended nucleic acid chains.

Rho and Primary Site RNA Interactions

Rho has two distinct nucleic acid binding sites. The primary mRNA binding sites are formed by the N-terminal domains, which have the ability to bind either single-stranded DNA or RNA (Galluppi and Richardson, 1980; Chen et al., 1986; McSwiggen et al., 1988; Modrak and Richardson, 1994). This feature was used to grow crystals of Rho in complex with target site mimics composed of either nucleic acid. Earlier studies have shown that each N-terminal domain binds a dinucleotide segment in a network of contacts that explain the preference of Rho for cytosine (Bogden et al., 1999). The first nucleotide base packs into a hydrophobic enclosure that is formed by the side chains of Tyr80, Glu108, and Tyr110, and is too small to comfortably hold purine bases. For the second nucleotide, the cytosine base stacks on the aromatic side chain of Phe64, while its O2, N3, and N4 groups interact with the side chains of the neighboring Arg66 and Asp78 (Bogden et al., 1999). No contacts are seen to the 2′ hydroxyl of the bound nucleic acid, explaining why Rho is able to bind both ssDNA and ssRNA.

In our full-length Rho complex, the primary RNA binding sites of the N-terminal domains lie equidistant from each other about the periphery of the hexamer. There

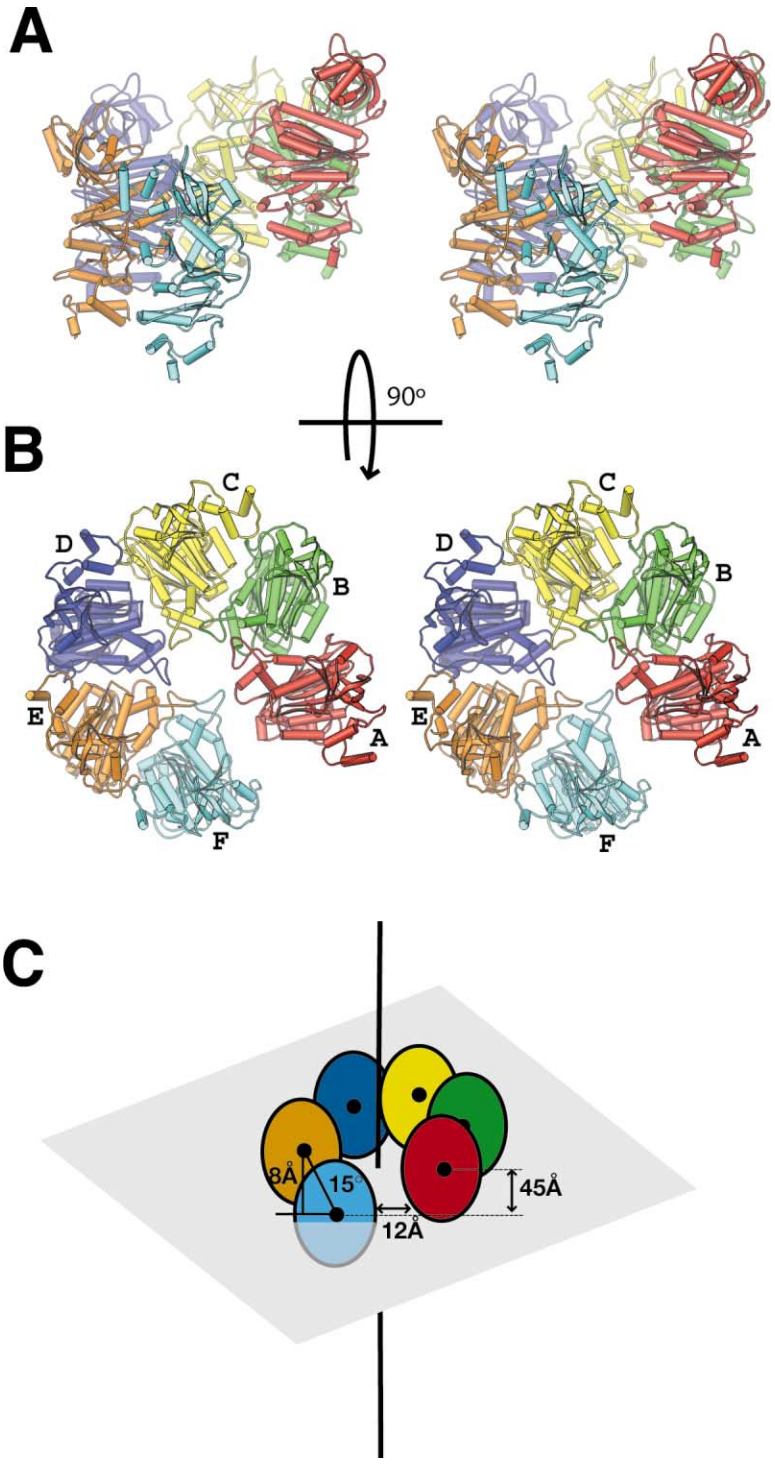

Figure 2. The Rho Hexamer

(A) Front view of the particle. The six subunits of Rho pack into an open hexameric ring. Each protomer is represented by a different color. The orientation of protomer C (yellow subunit) is similar to that shown in Figure 1A.

(B) Topdown view of (A). Protomers are labeled A–F.

(C) Schematic of the relative rise and offset of adjacent Rho subunits as they wind about the pseudo-6-fold axis of the ring (vertical line). Ovals are colored according to the color scheme in (A) and (B). The gap between monomers A and F is 12 Å, and the helical pitch is 45 Å.

is clear electron density for nucleic acid in the OB-fold binding cleft of five of the six N-terminal domains. The one N-terminal domain that lacks density for the DNA or RNA substrate belongs to protomer B; the helical bundle of this domain is also disordered. As anticipated, each binding site accommodates an oligo-(deoxy) cytadylic acid dinucleotide as seen for the isolated Rho N-terminal domain/RNA complex solved previously (Bogden et al., 1999). There is no observable electron density for nucleic acid outside of the primary binding site.

Surprisingly, the arrangement between the N- and C-terminal regions of each protomer is such that the primary RNA binding clefts face inward, toward the central hole of the ring (Figure 3A). This finding was unexpected, because earlier data had suggested that the primary mRNA binding cleft might reside on the outer periphery of the ring (Yu et al., 2000). Several lines of

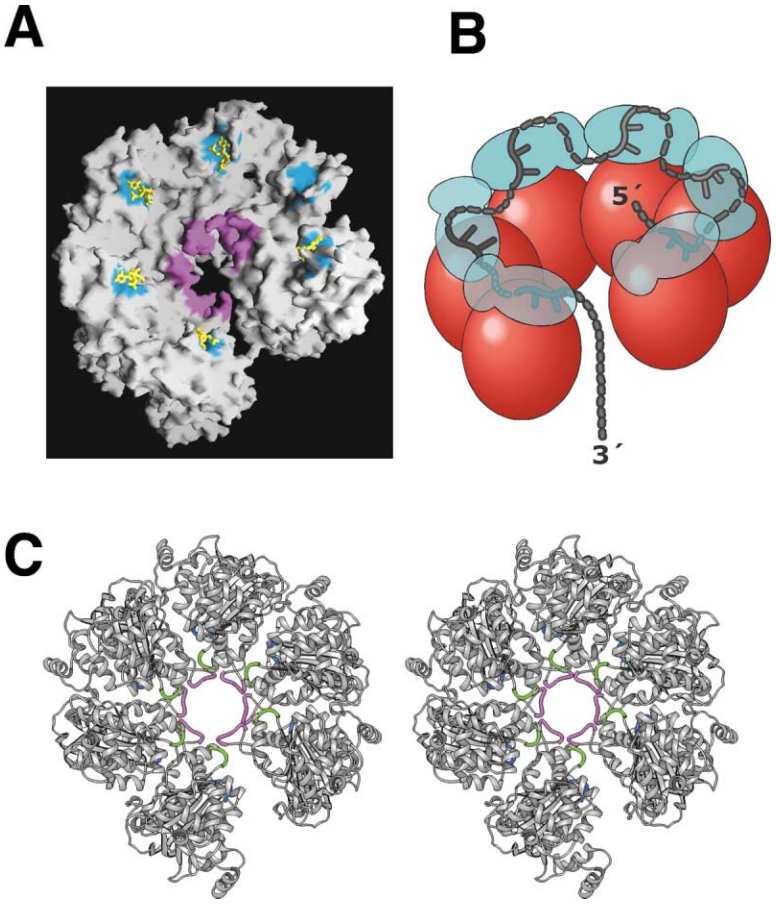

Figure 3. Rho RNA Binding Sites

(A) Molecular surface (GRASP [Nicholls et al., 1991]) of the Rho hexamer. Primary RNA binding sites in the OB-fold of the N-terminal domain are colored cyan. Secondary (C-terminal) RNA binding sites in the ATPase domain are colored magenta. Nucleic acid bound at the primary RNA binding sites is shown as yellow rods. View is the same as in Figure 2B.

(B) Schematic of the primary (N-terminal) RNA binding site configuration. The N- and C-terminal domains are colored green and red, respectively. Solid black lines represent the positions for the single-stranded nucleic acid, which binds across the primary RNA binding site and orients the 3′ end toward the hole of the ring. The broken black line shows the path needed to be traversed by nucleic acid between adjacent binding sites.

(C) Rho's secondary RNA binding site. Stereo diagram of the Rho hexamer showing the location of the P loops (blue), the Q loops (magenta) and the R loops (green). View is from the "bottom," rotated 180° from the perspective of Figure 2B.

evidence, however, indicate that the observed configuration represents the natural architecture of the Rho particle. First, each of the six protomers in the asymmetric unit independently adopts the same conformation and orientation. Second, there are extensive hydrophobic contacts between the N- and C-terminal domains, burying a total surface area of ~850 Å^2 per protomer (Figure 1B). Finally, this arrangement places the extended linker that connects the N- and C-terminal domains on the exterior of the ring, consistent with protease mapping experiments that have shown this region to be accessible and labile (Bear et al., 1985; Dolan et al., 1990).

The relative orientation of the N- and C-terminal domains has important consequences for RNA recognition. The primary RNA binding sites are arranged such that they bind substrate at an angle of 75° to a plane perpendicular to the pseudo 6-fold rotation axis of the ring. The substrate is oriented such that the 3′ end points down, toward the interior hole of the ring (Figure 3B). This configuration constrains the minimal distance between the 3′ and 5′ ends of successive RNA binding sites to be 35 Å. As a result, a 12–13 base RNA oligonucleotide would be minimally required to span two adjacent N-terminal domains and, in contrast to models suggesting that RNA might directly feed from one domain to another (Bogden et al., 1999), any RNA long enough to bridge two or more protomers would be forced to zigzag between the primary sites (Figure 3B). In total, the length of an ssRNA sufficient to span the entire N-terminal periphery of the ring would be approximately 70–80 bases, a value in excellent agreement with ribonuclease A digestion experiments of RNAs bound to the Rho hexamer (Bear et al., 1988; Zhu and von Hippel, 1998b, 1998a).

Rho and Secondary Site RNA Interactions

mRNA translocation and unwinding are thought to be catalyzed at Rho's secondary RNA binding site. This function depends on two sequence motifs known as the Q and R loops (Burgess and Richardson, 2001a; Wei and Richardson, 2001b, 2001a; Xu et al., 2002). Both loops, as predicted from a homology model based on the F_1 ATPase (Miwa et al., 1995; Burgess and Richardson, 2001a), line the interior hole of the hexamer. Each Q loop lies on the upper segment of the C-terminal domain and extends into the center of the ring. The constellation of the six Q loops in the hexamer together form the narrowest constriction (diameter 20 Å) of the interior hole (Figures 3A and 3C). Part of the Q loop of each protomer is disordered, reflecting the intrinsic mobility of this region, and may result from an absence of observable contacts with the nucleic acid substrate.

In contrast to the Q loops, the R loops are implicated in both ATP and RNA binding (Xu et al., 2002). Each R loop resides on a segment located at the subunit-subunit interface between the C-terminal domains, and lies both adjacent to and above the P loop of the ATP binding

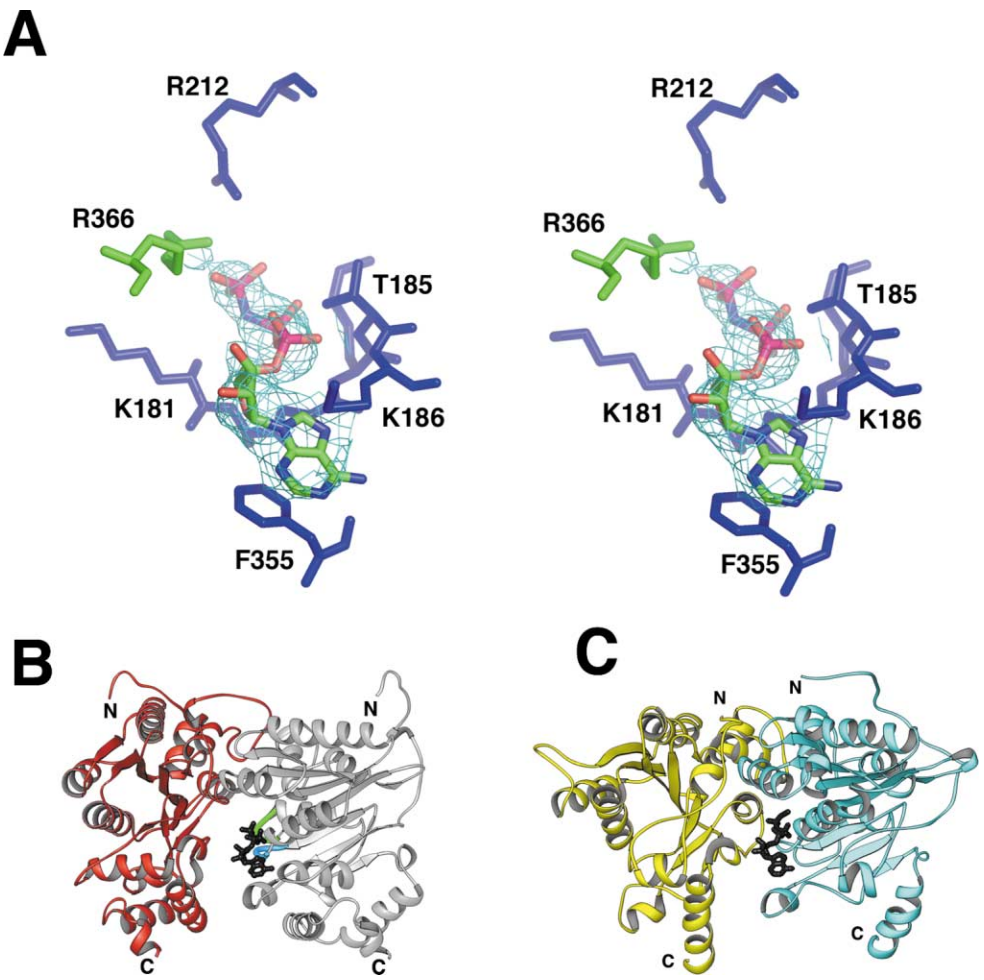

Figure 4. ATP Associations

(A) Stereo view of specific Rho and AMP-PNP interactions. F_o-F_c electron density contoured at 2σ is shown for the bound nucleotide. Residues important for nucleotide binding and hydrolysis are shown in ball and stick. Residues from two adjacent C-terminal domains form the active site and are colored blue and green.

(B) Rho nucleotide binding pocket conformation. The two adjacent C-terminal domains are colored red and gray (protomers D and E). The active site is partly closed and can bind nucleotide, but does not appear fully organized to carry out hydrolysis. The P loop (blue) is shown next to the R loop motif (green).

(C) F_1 ATPase nucleotide binding pocket conformation (1bmf). Two ATPase domains are colored yellow and cyan, and bound nucleotide is shown as black rods. The active site cleft is fully closed and competent to carry out nucleotide hydrolysis.

pocket (Figures 3C and 4B). Part of each R loop also lines the interior hole of the Rho hexamer. The position of the R loop and its contact with the P loop indicates that this motif could function as part of an allosteric effector switch that directly couples RNA binding in the hole of the hexamer to the ATP binding and hydrolysis site (Richardson and Conaway, 1980; Shigesada and Wu, 1980; Richardson, 1982; Engel and Richardson, 1984; Kim and Patel, 2001). Consistent with this hypothesis, RNA binding to the secondary state coincides with closure of the hexameric ring and stimulation of the ATPase activity (Gogol et al., 1991; Gan and Richardson, 1999), presumably by introducing conformational changes between subunits and residues around the ATP binding site (Lowery-Goldhammer and Richardson, 1974). It is interesting to note that the positioning of the primary RNA binding sites places the 3′ RNA end near the secondary sites from the outset of mRNA binding, explaining why RNA appears to be readily captured for translocation following primary site occupancy (Kim and Patel, 2001).

Nucleotide Associations and Rho Function

The ATP binding pocket of Rho is located at the interface between the C-terminal domains of adjacent protomers (Figure 4B). Part of this region is formed by signature sequence motifs such as the adjacent Walker-A (GXGXXGK(S/T) and Walker-B (D(D/E)XX) segments. For native crystals grown in the presence of AMPPNP, clear electron density for bound nucleotide is seen in all six ATP binding pockets of the hexameric ring (Figure 4A). In contrast, weak electron density is observed for nucleotide in the structure determined with the selenomethionine protein, indicating that the occupancy at this site is low. This difference appears due to the insertion of the hydrophobic side chain SeMet186 of the seleno-

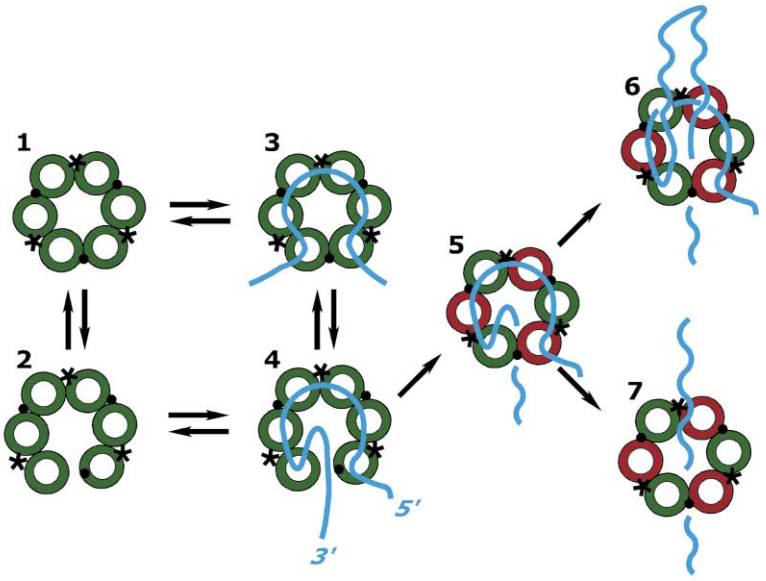

Figure 5. Schematic Model for Rho Function

Numbers correspond to stages outlined in the text. Asterisks represent catalytic sites thought to be competent for ATP hydrolysis.

methionine protein into the adenine binding pocket of each of the six subunits. Nonetheless, superposition of the ATP bound and -free structures shows that the organization and conformation of the ATP binding sites are the same.

Cocrystallization (as opposed to soaking) of Rho with AMPPNP shows that nucleotide can associate with an open-ring state of the protein. The interactions between Rho and the adenosine base of bound AMPPNP are typical of those seen for other RecA-type proteins, in which aliphatic or aromatic side chains sandwich the purine moiety in a "hydrophobic pincer" (Figure 4A) (Boyer, 1997; Bird et al., 1998a; Singleton et al., 2000; Xu et al., 2000). Other nucleotide associations are not canonical, however. For example, residues in the Walker-A and -B regions do not make standard contacts to the β- and γ-phosphates of AMPPNP, nor is magnesium evident in our structure (Figure 4A). These altered features arise because the subunit-subunit orientation of the open ring splays apart the ATPase domains as compared to other RecA-type proteins that have formed competent active sites (Figures 4B and 4C). Given that the open-ring form of Rho imaged here appears consistent with an mRNA loading state, as opposed to an actively translocating helicase, such atypical nucleotide associations are perhaps not surprising, although these data indicate that ring opening can still occur when Rho is bound to ATP, as would be expected when the protein operates in vivo.

Rho Architecture and Mechanistic Implications

As a collective, the structures observed here explain several important features of Rho function. First, Rho's primary RNA binding sites line the perimeter of the hexamer and face inward toward the center of the particle. Second, the primary sites orient the 3′ end of nucleic acid target sequences into the interior hole, which is formed by motifs known to be critical for coupling mRNA translocation and unwinding to ATP turnover. Third, the ring of the hexamer is split by a gap ~12 Å wide, providing both an entry point into what would otherwise be the topologically confined interior of the ring and suggesting a means by which the protein may enter a nucleic acid "loading" configuration. This general organization provides an elegant means to ensure that target mRNAs are efficiently captured by the protein, thereby activating the particle and initiating the process of transcription termination.

The significance of the Rho open-ring state may be applicable to other toroidal helicases and translocases. A long-standing puzzle has been to understand how extended nucleic acid segments gain entry to the interior of such protein rings, where unwinding and translocation are thought to occur. Many helicases, such as DnaB, papilloma virus E1, and the MCM complex, use specialized loading proteins to accomplish this task (Lusky et al., 1993; Seo et al., 1993; Donovan et al., 1997; Tanaka et al., 1997; Weinreich et al., 1999; Barcena et al., 2001). Others, such as Rho, appear to load onto target substrates without accessory factors. The ability of Rho to spontaneously switch between open- and closed-ring structures provides an immediate solution to the loading problem (Gogol et al., 1991; Yu et al., 2000; Richardson, 2002). By utilizing intersubunit hinging motions evident in a number of RecA-type ATPases, our structure shows how Rho can configure the relative orientation of neighboring RecA-type folds to allow ring opening without fully exposing subunit interfaces that might otherwise foster filamentation. As a result, the Rho model may be applicable for understanding how other ring systems are breached to bind nucleic acids, and may potentially represent a structural state accessed for some helicases through loader protein activity.

Another interesting finding is that the Rho hexamer can remain open and, thus, competent to bind mRNA at its secondary binding sites even when Rho's ATP and primary mRNA binding sites are occupied. This observation allows us to expand upon models explaining how Rho recognizes *rut* sites and loads onto RNA in vivo (Richardson, 2002; Delagoutte and von Hippel, 2003). Extensive previous work, together with our structural

data, suggest that Rho can oscillate between closed- and open-ring states, either of which may associate with ATP and target mRNAs (Figure 5, stages 1 and 2). In the open state, ATP would be loosely associated with Rho and only partially liganded as observed here. In contrast, entry into the closed state would properly position and coordinate nucleotide for hydrolysis. Natural conversion between the two structural states would allow ATP hydrolysis to be observed in the absence of RNA (Stitt, 2001), but turnover would not be fully activated, both because of the lack of RNA effector signals through the Q and R loops and because a population of Rho molecules might be open at any given moment.

Loading and priming of Rho would begin through the association of a *rut* site with the primary RNA binding sites in the N-terminal domains. The configuration of the N-terminal domains automatically orients the 3′ end of message toward the interior hole of the protein. Were the ring to be open during *rut* site binding, mRNA could simply thread its way through the gap between monomers and into the interior of the hexamer to associate with the secondary RNA binding sites (Figure 5, stage 4). In contrast, if the ring were closed upon *rut* site recognition (Figure 5, stage 3), mRNA entry would need to wait until the ring spontaneously opens. It remains a possibility that mRNA binding to the primary, N-terminal domain binding sites might directly favor ring opening (Yu et al., 2000; Kim and Patel, 2001).

Once bound in the interior, RNA would be sensed by the Q and R loop regions, allosterically activating Rho and converting the protein into a stable, closed configuration (Figure 5, stage 5). Based on comparisons with closed-ring RecA-type proteins, ring closure would presumably occur through conformational changes between a subset of the ATPase domains, both forming competent set of active sites and compensating for the 15° subunit-subunit angular rise observed for the open-ring form. Ensuing cycles of ATP turnover would serve to modulate the relative orientation of neighboring ATPase domains, providing directed structural changes to propel the protein 5′→3′ along the message (Brennan et al., 1987; Singleton et al., 2000). As translocation begins, Rho could either dissociate from the *rut* site or could remain bound to the target motif as predicted by the tethered tracking model (Figure 5, stages 6 and 7). Although our structure cannot rule out either mechanism, it is interesting to note that the N-terminal domains open out from the center of the ring, creating a wide depression across the top of the particle. The size of this depression appears ample enough to remain associated with a RNA segment while single-stranded RNA is spooled away from the protein during translocation. Future efforts focused toward assembling RNA bound, closed ring structures will be needed to help distinguish between these models and to better illuminate the physical coupling between ATP usage, translocation, and unwinding.

Experimental Procedures

Protein Expression and Purification

The open reading frame encoding the full-length *Escherichia coli* Rho protein was PCR amplified and cloned into pET24b. The plasmid was transformed into the *Escherichia coli* strain BL21 (pLysS), and the native protein overexpressed in 2XYT media by induction at an OD_{600} of 0.3–0.5 with 1 mM IPTG at 37°C for 3 hr. Cells were lysed by sonication in 50 mM Tris-HCl (pH 7.5), 10% glycerol, 50 mM KCl, 1 mM TCEP (Tris(2-carboxyethyl)phosphine hydrochloride) on ice. The protein was twice purified over a POROS-HS column (Perseptive Biosystems) then further purified with two successive Sephacryl S-300 (Amersham) sizing columns in 10 mM Tris-HCl (pH 7.5), 50 mM NaCl, and 1 mM TCEP. The protein at this stage was more than 99% pure as judged by SDS-PAGE and Coomassie staining and was monodisperse as judged by dynamic light scattering (DynaPro, model 99-CP, Protein Solutions). Protein was concentrated by ultrafiltration (Centriprep-10, Amicon) to 15 mg/ml. Selenomethionine protein was overexpressed in minimal media using the protocol of Van Duyne and coworkers (Van Duyne et al., 1993) and was purified similar to native Rho.

Crystallization and Data Collection

Initial crystals of full-length Rho diffracted poorly. Cocrystals with DNA or RNA substrates resulted in crystals of different morphology to those obtained in the absence of nucleic acid and proved instrumental in solving the Rho structure. A number of single-stranded DNA and RNA substrates were tested in cocrystallization trials. DNAs and RNAs varied in length (6–19 bases) and composition (one or two binding sites), and were designed based on Rho's specificity for the unstructured, cytosine-rich mRNA regions present in *rut* sites. The best quality crystals in terms of size, stability, and diffraction were those cocrystallized with a 15-mer DNA substrate (AACC CAAGAACCCAA) or with an 8-mer RNA substrate $(CU)_4$.

Cocrystals of Rho in complex with the single-stranded DNA substrate were grown by vapor diffusion at room temperature. Stock protein solutions were dialyzed in 10 mM Tris-HCl (pH 7.5) and 50 mM NaCl at 4°C prior to crystallization. One volume of protein solution was mixed with one volume of crystallization solution containing 100 mM Na•Cacodylate (pH 6.5), 100 mM NaCl, 5% PEG 8K, 40% glycerol, 0.6 mM n-Nonyl-β-D-thiomaltoside, and 2 mM TCEP; the well solution was diluted with an equivalent amount of H_2O prior to sealing the drop over the reservoir. Small crystals appeared overnight and grew to average dimensions of 100 × 100 × 200 μM in 1 week. Crystals were introduced into cryoprotectant, containing a mix of 50 mM Tris-HCl (pH 7.5), 50 mM NaCl, 3% PEG 8K, 25% glycerol, and 5% PEG 400, in a fast, single step, then flash frozen in liquid nitrogen. The crystals belong to the monoclinic space group C2 with unit cell dimensions of a = 119.2 Å, b = 205.8 Å, c = 148.0 Å, and β = 95.3°. There is one hexamer per asymmetric unit.

Structure Determination and Refinement

All data were collected at Beamline 8.3.1 at the Advanced Light Source (ALS) using an ADSC Quantum-Q210 CCD detector. Diffraction data were processed using DENZO and SCALEPACK (Otwinowski, 1997) (Table 1). Initial attempts to calculate phases using selenomethionine MAD or SAD experiments were unsuccessful, so a tantalum derivative was prepared by soaking a crystal overnight with saturated solution of $Ta_6Br_{12}^{2+}$. Heavy atom positions were identified by SOLVE (Terwilliger and Berendzen, 1999), and MLPHARE (CCP4, 1994) was used to calculate initial phases to 6.0 Å based on isomorphous and anomalous differences for this derivative (Table 1). Selenium sites (83 out of 96) were located by calculating anomalous difference maps to 3.6 Å resolution using the tantalum phases (Table 1). The selenium sites were refined initially with MLPHARE and then with SHARP (de la Fortelle and Bricogne, 1997), followed by DM solvent flattening (Cowtan, 1994) to yield starting electron density maps.

Five out of the six N-terminal domains were located in the solvent-flattened density by the program FFFEAR (Cowtan K., 1998) using the X-ray model 2a8v (Bogden et al., 1999). The sixth domain was placed into the map manually and the fit optimized using RSR-RIGID in O (Jones T.A., 1991). The N-terminal domains were used to derive the six NCS (noncrystallographic symmetry) operators within the asymmetric unit and the experimental electron density map was subsequently improved using solvent flattening with NCS multidomain averaging and phase extension in DM. The C-terminal domain of the mitochondrial F_1 ATPase model (1bmf) was manually docked and rebuilt into this DM-averaged density using O.

The model was refined with REFMAC5 (Murshudov G.N., 1997), using ARP (Lamzin and Wilson, 1993) for water building. In the final cycles of refinement, TLS (translation libration and screw-rotation) refinement of rigid groups (Winn et al., 2001) was carried out as implemented in REFMAC5 (Table 2). The refined selenomethionine Rho/DNA structure was used to solve the native Rho/RNA•AMPPNP complex by molecular replacement using the program AMORE (Navaza, 2001). The resultant solution was DM solvent flattened and multidomain averaged, revealing clear electron density in F_o-F_c maps for AMPPNP in all six ATP binding sites. The structure was then refined using REFMAC5. The Rho/DNA and the Rho/RNA structures were refined to a final R_{work} 27.0% and 27.0% and an R_{free} 29.6% and 30.3%, respectively. A total of 2472 out of 2502 residues are accounted for in either of the two structures (Table 2). Geometric analysis were carried out with Procheck (Laskowski et al., 1993) and structural superpositions with LSQKAB (CCP4, 1994).

Acknowledgments

The authors are grateful to James Holton at Beamline 8.3.1 of the Advanced Light source for assistance with data acquisition and to David King for mass spectroscopy analyses. We would also like to thank James Keck, Deborah Fass, David Akey, Jan Erzberger, and Scott Gradia for critical reading the manuscript, as well as members of the Berger Lab for helpful discussions and insights. This work was supported by generous assistance from the G. Harold and Leila Y. Mathers Charitable Foundation.

Received: March 19, 2003
Revised: May 20, 2003
Accepted: June 25, 2003
Published: July 10, 2003

References

Abrahams, J.P., Leslie, A.G., Lutter, R., and Walker, J.E. (1994). Structure at 2.8 Å resolution of F1-ATPase from bovine heart mitochondria. Nature *370*, 621–628.

Alifano, P., Rivellini, F., Limauro, D., Bruni, C.B., and Carlomagno, M.S. (1991). A consensus motif common to all Rho-dependent prokaryotic transcription terminators. Cell *64*, 553–563.

Allison, T.J., Wood, T.C., Briercheck, D.M., Rastinejad, F., Richardson, J.P., and Rule, G.S. (1998). Crystal structure of the RNA-binding domain from transcription termination factor rho. Nat. Struct. Biol. *5*, 352–356.

Barcena, M., Ruiz, T., Donate, L.E., Brown, S.E., Dixon, N.E., Radermacher, M., and Carazo, J.M. (2001). The DnaB.DnaC complex: a structure based on dimers assembled around an occluded channel. EMBO J. *20*, 1462–1468.

Bear, D.G., Andrews, C.L., Singer, J.D., Morgan, W.D., Grant, R.A., von Hippel, P.H., and Platt, T. (1985). Escherichia coli transcription termination factor rho has a two-domain structure in its activated form. Proc. Natl. Acad. Sci. USA *82*, 1911–1915.

Bear, D.G., Hicks, P.S., Escudero, K.W., Andrews, C.L., McSwiggen, J.A., and von Hippel, P.H. (1988). Interactions of Escherichia coli transcription termination factor rho with RNA. II. Electron microscopy and nuclease protection experiments. J. Mol. Biol. *199*, 623–635.

Bird, L.E., Brannigan, J.A., Subramanya, H.S., and Wigley, D.B. (1998a). Characterisation of Bacillus stearothermophilus PcrA helicase: evidence against an active rolling mechanism. Nucleic Acids Res. *26*, 2686–2693.

Bird, L.E., Subramanya, H.S., and Wigley, D.B. (1998b). Helicases: a unifying structural theme? Curr. Opin. Struct. Biol. *8*, 14–18.

Bogden, C.E., Fass, D., Bergman, N., Nichols, M.D., and Berger, J.M. (1999). The structural basis for terminator recognition by the Rho transcription termination factor. Mol. Cell *3*, 487–493.

Boyer, P.D. (1997). The ATP synthase–a splendid molecular machine. Annu. Rev. Biochem. *66*, 717–749.

Brennan, C.A., Dombroski, A.J., and Platt, T. (1987). Transcription termination factor rho is an RNA-DNA helicase. Cell *48*, 945–952.

Brennan, C.A., Steinmetz, E.J., Spear, P., and Platt, T. (1990). Specificity and efficiency of rho-factor helicase activity depends on magnesium concentration and energy coupling to NTP hydrolysis. J. Biol. Chem. *265*, 5440–5447.

Briercheck, D.M., Wood, T.C., Allison, T.J., Richardson, J.P., and Rule, G.S. (1998). The NMR structure of the RNA binding domain of E. coli rho factor suggests possible RNA-protein interactions. Nat. Struct. Biol. *5*, 393–399.

Brown, S., Brickman, E.R., and Beckwith, J. (1981). Blue ghosts: a new method for isolating amber mutants defective in essential genes of Escherichia coli. J. Bacteriol. *146*, 422–425.

Burgess, B.R., and Richardson, J.P. (2001a). RNA passes through the hole of the protein hexamer in the complex with the Escherichia coli Rho factor. J. Biol. Chem. *276*, 4182–4189.

Burgess, B.R., and Richardson, J.P. (2001b). Transcription factor Rho does not require a free end to act as an RNA-DNA helicase on an RNA. J. Biol. Chem. *276*, 17106–17110.

Cavarelli, J., Rees, B., Ruff, M., Thierry, J.C., and Moras, D. (1993). Yeast tRNA(Asp) recognition by its cognate class II aminoacyl-tRNA synthetase. Nature *362*, 181–184.

CCP4 (Collaborative Computational Project 4) (1994). The CCP4 suite: programs for protein crystallography. Acta Crystallogr. D *50*, 760–763.

Chen, C.Y., Galluppi, G.R., and Richardson, J.P. (1986). Transcription termination at lambda tR1 is mediated by interaction of rho with specific single-stranded domains near the 3′ end of cro mRNA. Cell *46*, 1023–1028.

Cowtan, K. (1994). A CCP4 density modification package. Joint CCP4 ESF-EACBM. Newslett. Prot. Crystallogr. *31*, 34–38.

Cowtan, K. (1998). Modified phased translation functions and their application to molecular fragment location. Acta Crystallogr. D *54*, 750–756.

de la Fortelle, E., and Bricogne, G. (1997). Maximum-likelihood heavy atom parameter refinement for multiple isomorphous replacement and multiwavelength anomalous diffraction methods. Methods Enzymol. *276*, 472–494.

Delagoutte, E., and von Hippel, P.H. (2003). Helicase mechanisms and the coupling of helicases within macromolecular machines. Part II: integration of helicases into cellular processes. Q. Rev. Biophys. *36*, 1–69.

Dolan, J.W., Marshall, N.F., and Richardson, J.P. (1990). Transcription termination factor rho has three distinct structural domains. J. Biol. Chem. *265*, 5747–5754.

Donovan, S., Harwood, J., Drury, L.S., and Diffley, J.F. (1997). Cdc6p-dependent loading of Mcm proteins onto pre-replicative chromatin in budding yeast. Proc. Natl. Acad. Sci. USA *94*, 5611–5616.

Engel, D., and Richardson, J.P. (1984). Conformational alterations of transcription termination protein rho induced by ATP and by RNA. Nucleic Acids Res. *12*, 7389–7400.

Galluppi, G.R., and Richardson, J.P. (1980). ATP-induced changes in the binding of RNA synthesis termination protein Rho to RNA. J. Mol. Biol. *138*, 513–539.

Gan, E., and Richardson, J.P. (1999). ATP and other nucleotides stabilize the Rho-mRNA complex. Biochemistry *38*, 16882–16888.

Geiselmann, J., Yager, T.D., and von Hippel, P.H. (1992). Functional interactions of ligand cofactors with Escherichia coli transcription termination factor rho. II. Binding of RNA. Protein Sci. *1*, 861–873.

Geiselmann, J., Wang, Y., Seifried, S.E., and von Hippel, P.H. (1993). A physical model for the translocation and helicase activities of Escherichia coli transcription termination protein Rho. Proc. Natl. Acad. Sci. USA *90*, 7754–7758.

Gogol, E.P., Seifried, S.E., and von Hippel, P.H. (1991). Structure and assembly of the Escherichia coli transcription termination factor rho and its interaction with RNA. I. Cryoelectron microscopic studies. J. Mol. Biol. *221*, 1127–1138.

Jones, T.A., Zou, J.Y., Cowan, S.W., and Kjeldgaard, M. (1991). Improved methods for building protein models in electron density

maps and the location of errors in these models. Acta Crystallogr. A *47*, 110–119.

Kim, D.E., and Patel, S.S. (2001). The kinetic pathway of RNA binding to the Escherichia coli transcription termination factor Rho. J. Biol. Chem. *276*, 13902–13910.

Lamzin, V.S., and Wilson, K.S. (1993). Automated refinement of protein models. Acta Crystallogr. D *49*, 129–147.

Laskowski, A.R., MacArthur, W.M., Moss, S.D., and Thornton, M.J. (1993). PROCHECK: a program to check the stereochemical quality of protein structures. J. Appl. Cryst. *26*, 283–291.

Lowery-Goldhammer, C., and Richardson, J.P. (1974). An RNA-dependent nucleoside triphosphate phosphohydrolase (ATPase) associated with rho termination factor. Proc. Natl. Acad. Sci. USA *71*, 2003–2007.

Lusky, M., Hurwitz, J., and Seo, Y.S. (1993). Cooperative assembly of the bovine papilloma virus E1 and E2 proteins on the replication origin requires an intact E2 binding site. J. Biol. Chem. *268*, 15795–15803.

Martinez, A., Burns, C.M., and Richardson, J.P. (1996a). Residues in the RNP1-like sequence motif of Rho protein are involved in RNA-binding affinity and discrimination. J. Mol. Biol. *257*, 909–918.

Martinez, A., Opperman, T., and Richardson, J.P. (1996b). Mutational analysis and secondary structure model of the RNP1-like sequence motif of transcription termination factor Rho. J. Mol. Biol. *257*, 895–908.

McSwiggen, J.A., Bear, D.G., and von Hippel, P.H. (1988). Interactions of Escherichia coli transcription termination factor rho with RNA. I. Binding stoichiometries and free energies. J. Mol. Biol. *199*, 609–622.

Miwa, Y., Horiguchi, T., and Shigesada, K. (1995). Structural and functional dissections of transcription termination factor rho by random mutagenesis. J. Mol. Biol. *254*, 815–837.

Modrak, D., and Richardson, J.P. (1994). The RNA-binding domain of transcription termination factor rho: isolation, characterization, and determination of sequence limits. Biochemistry *33*, 8292–8299.

Morgan, W.D., Bear, D.G., and von Hippel, P.H. (1983). Rho-dependent termination of transcription. I. Identification and characterization of termination sites for transcription from the bacteriophage lambda PR promoter. J. Biol. Chem. *258*, 9553–9564.

Morgan, W.D., Bear, D.G., Litchman, B.L., and von Hippel, P.H. (1985). RNA sequence and secondary structure requirements for rho-dependent transcription termination. Nucleic Acids Res. *13*, 3739–3754.

Murshudov G.N., Vagin, A.A., and Dodson, E.J. (1997). Refinement of macromolecular structures by the maximum-likelihood method. Acta Crystallogr. D *53*, 240–255.

Navaza, J. (2001). Implementation of molecular replacement in AMoRe. Acta Crystallogr. D Biol. Crystallogr. *57*, 1367–1372.

Newkirk, K., Feng, W., Jiang, W., Tejero, R., Emerson, S.D., Inouye, M., and Montelione, G.T. (1994). Solution NMR structure of the major cold shock protein (CspA) from Escherichia coli: identification of a binding epitope for DNA. Proc. Natl. Acad. Sci. USA *91*, 5114–5118.

Nicholls, A., Sharp, K.A., and Honig, B. (1991). Protein folding and association: insights from the interfacial and thermodynamic properties of hydrocarbons. Proteins *11*, 281–296.

Oda, T., and Takanami, M. (1972). Observations on the structure of the termination factor rho and its attachment to DNA. J. Mol. Biol. *71*, 799–802.

Opperman, T., and Richardson, J.P. (1994). Phylogenetic analysis of sequences from diverse bacteria with homology to the Escherichia coli rho gene. J. Bacteriol. *176*, 5033–5043.

Otwinowski, Z., and Minor, W. (1997). Processing of X-ray diffraction data collected in oscillation mode. Methods Enzymol. *276*, 307–326.

Platt, T. (1994). Rho and RNA: models for recognition and response. Mol. Microbiol. *11*, 983–990.

Richardson, J. (2002). Rho-dependent termination and ATPases in transcript termination. Biochim. Biophys. Acta *1577*, 251–260.

Richardson, J.P. (1982). Activation of rho protein ATPase requires simultaneous interaction at two kinds of nucleic acid-binding sites. J. Biol. Chem. *257*, 5760–5766.

Richardson, J.P., and Conaway, R. (1980). Ribonucleic acid release activity of transcription termination protein rho is dependent on the hydrolysis of nucleoside triphosphates. Biochemistry *19*, 4293–4299.

Richardson, J.P., and Greenblatt, J. (1996). Escherichia coli and salmonella. In Cellular and Molecular Biology, Second Edition, F.C. Neidhardt, R. Curtiss III, J.L. Ingraham, E.C.C. Lin, K.B. Low, B. Magasanik, W.S. Reznikoff, M. Riley, M. Schaechter, and H.E. Umbarger, eds. (Washington, D.C.: American Society for Microbiology), pp. 822–848.

Richardson, L.V., and Richardson, J.P. (1992). Cytosine nucleoside inhibition of the ATPase of Escherichia coli termination factor rho: evidence for a base specific interaction between rho and RNA. Nucleic Acids Res. *20*, 5383–5387.

Roberts, J.W. (1969). Termination factor for RNA synthesis. Nature *224*, 1168–1174.

Sawaya, M.R., Guo, S., Tabor, S., Richardson, C.C., and Ellenberger, T. (1999). Crystal structure of the helicase domain from the replicative helicase-primase of bacteriophage T7. Cell *99*, 167–177.

Schindelin, H., Jiang, W., Inouye, M., and Heinemann, U. (1994). Crystal structure of CspA, the major cold shock protein of Escherichia coli. Proc. Natl. Acad. Sci. USA *91*, 5119–5123.

Seo, Y.S., Muller, F., Lusky, M., Gibbs, E., Kim, H.Y., Phillips, B., and Hurwitz, J. (1993). Bovine papilloma virus (BPV)-encoded E2 protein enhances binding of E1 protein to the BPV replication origin. Proc. Natl. Acad. Sci. USA *90*, 2865–2869.

Shigesada, K., and Wu, C.W. (1980). Studies of RNA release reaction catalyzed by E. coli transcription termination factor rho using isolated ternary transcription complexes. Nucleic Acids Res. *8*, 3355–3369.

Singleton, M.R., Sawaya, M.R., Ellenberger, T., and Wigley, D.B. (2000). Crystal structure of T7 gene 4 ring helicase indicates a mechanism for sequential hydrolysis of nucleotides. Cell *101*, 589–600.

Steinmetz, E.J., and Platt, T. (1994). Evidence supporting a tethered tracking model for helicase activity of Escherichia coli Rho factor. Proc. Natl. Acad. Sci. USA *91*, 1401–1405.

Stitt, B.L. (2001). Escherichia coli transcription termination factor Rho binds and hydrolyzes ATP using a single class of three sites. Biochemistry *40*, 2276–2281.

Story, R.M., Weber, I.T., and Steitz, T.A. (1992). The structure of the E. coli recA protein monomer and polymer. Nature *355*, 318–325.

Sullivan, S.L., and Gottesman, M.E. (1992). Requirement for E. coli NusG protein in factor-dependent transcription termination. Cell *68*, 989–994.

Tanaka, T., Knapp, D., and Nasmyth, K. (1997). Loading of an Mcm protein onto DNA replication origins is regulated by Cdc6p and CDKs. Cell *90*, 649–660.

Terwilliger, T.C., and Berendzen, J. (1999). Automated MAD and MIR structure solution. Acta Crystallogr. D *55*, 849–861.

Van Duyne, G.D., Standaert, R.F., Karplus, P.A., Schreiber, S.L., and Clardy, J. (1993). Atomic structures of the human immunophilin FKBP-12 complexes with FK506 and rapamycin. J. Mol. Biol. *229*, 105–124.

von Hippel, P.H., and Delagoutte, E. (2001). A general model for nucleic acid helicases and their "coupling" within macromolecular machines. Cell *104*, 177–190.

Walstrom, K.M., Dozono, J.M., Robic, S., and von Hippel, P.H. (1997). Kinetics of the RNA-DNA helicase activity of Escherichia coli transcription termination factor rho. 1. Characterization and analysis of the reaction. Biochemistry *36*, 7980–7992.

Wei, R.R., and Richardson, J.P. (2001a). Identification of an RNA-binding Site in the ATP binding domain of Escherichia coli Rho by H2O2/Fe-EDTA cleavage protection studies. J. Biol. Chem. *276*, 28380–28387.

Wei, R.R., and Richardson, J.P. (2001b). Mutational changes of conserved residues in the Q-loop region of transcription factor Rho greatly reduce secondary site RNA-binding. J. Mol. Biol. *314*, 1007–1015.

Weinreich, M., Liang, C., and Stillman, B. (1999). The Cdc6p nucleotide-binding motif is required for loading mcm proteins onto chromatin. Proc. Natl. Acad. Sci. USA *96*, 441–446.

Winn, M.D., Isupov, M.N., and Murshudov, G.N. (2001). Use of TLS parameters to model anisotropic displacements in macromolecular refinement. Acta Crystallogr. D *57*, 122–133.

Xu, H., Frank, J., Niedenzu, T., and Saenger, W. (2000). DNA helicase RepA: cooperative ATPase activity and binding of nucleotides. Biochemistry *39*, 12225–12233.

Xu, Y., Kohn, H., and Widger, W.R. (2002). Mutations in the rho transcription termination factor that affect RNA tracking. J. Biol. Chem. *277*, 30023–30030.

Yu, X., Horiguchi, T., Shigesada, K., and Egelman, E.H. (2000). Three-dimensional reconstruction of transcription termination factor rho: orientation of the N-terminal domain and visualization of an RNA-binding site. J. Mol. Biol. *299*, 1279–1287.

Zhu, A.Q., and von Hippel, P.H. (1998a). Rho-dependent termination within the trp t' terminator. I. Effects of rho loading and template sequence. Biochemistry *37*, 11202–11214.

Zhu, A.Q., and von Hippel, P.H. (1998b). Rho-dependent termination within the trp t' terminator. II. Effects of kinetic competition and rho processivity. Biochemistry *37*, 11215–11222.

Accession Numbers

Coordinates for both Rho complexes have been deposited in the RCSB PDB database and are available under the accession codes 1PV4 and 1PVO.